Signal, Image and Video Processing (2018) 12:1361–1367
https://doi.org/10.1007/s11760-018-1290-0

ORIGINAL PAPER

A sparsity-based Bayesian approach for hyperspectral unmixing using normal compositional model

F. Amiri[1] · M. H. Kahaei[1]

Received: 25 October 2016 / Revised: 16 April 2018 / Accepted: 22 April 2018 / Published online: 2 May 2018

Abstract
A new Bayesian-based method is developed for unmixing of hyperspectral images. Endmembers are assumed variable based on the Gaussian distribution. A semi-supervised scenario is considered, and as a practical aspect, the abundance vectors are assumed sparse. We propose the Dirichlet prior to represent the sparsity and derive the corresponding posteriors in Bayesian sense. Numerical results are used to evaluate different methods for both simulated and real data. It is shown that the proposed method achieves a lower error in abundance estimation and image reconstruction.

Keywords Hyperspectral unmixing · Endmember variability · Bayesian · Normal compositional model · Sparse representation

1 Introduction

Hyperspectral images (HSI's) constitute the main database for remote sensing problems [1] such as agricultural and environmental monitoring [2], mineral exploration [3], and military surveillance [4]. In the HSI, each pixel is presented by a three-dimensional data cube whose third dimension contains the spectral information. To do so, the hyperspectral cameras collect 2-D spatial photographs over many adjacent spectral bands commonly containing the visible, near-infrared, and shortwave infrared spectral bands in the range 0.35–2.5 μm [2]. However, due to the low spatial resolution of imaging sensors, each single pixel represents a mixture of different materials located in the field of view [5]. In some applications of remote sensing, we are interested in identifying the materials involved in each pixel which motivates more research on unmixing techniques. For this purpose, each pixel of hyperspectral images is decomposed into a group of pure spectral signatures and their corresponding proportions, known as endmembers and abundances, respectively [6]. In practice, this is performed under two physical limitations on abundances, i.e., the non-negativity and sum-to-one constraints. From the first one, the mean of each abundance vector should be larger than zero, while the second constraint implies that the sum of abundance fractions should be equal to one. Moreover, an encountered difficulty that arises in unmixing problems is variability of the measured spectral signatures of endmembers which is due to the unstable atmospheric, illumination, and temporal conditions [7]. A number of methods have addressed the spectral variability [8] among which the multiple endmember spectral mixture analysis (MESMA) is well known [7]. However, when the spectral library becomes large, the MESMA leads to extremely large computations due to the requirement of exhaustive search over all possible combinations of endmembers. The support vector machines (SVMs) have also been incorporated for spectral unmixing with addressing spectral variations [9].

On the other hand, the endmember spectral variability may be modeled statistically using the Gaussian and beta distributions. Accordingly, the normal compositional model (NCM) and beta compositional model (BCM) [10,11], and also Bayesian estimators are developed. To do so, the uniform prior has already been considered over a set of proportion values that satisfy the non-negativity and sum-to-one constraints [10–13]. However, this prior is essentially more suitable for supervised unmixing scenarios, in which exact endmembers are assumed known. In contrast, in the semi-supervised unmixing problems, a few endmembers are chosen from a large spectral dictionary and thus the abundance vector is assumed sparse. Although the sparse property along with the endmember variability condition has already been studied for

✉ M. H. Kahaei
kahaei@iust.ac.ir

[1] School of Electrical Engineering, Iran University of Science and Technology, Tehran, Iran

reducing the unmixing error [14–17], still developing more drastic tools is of interest to researchers.

In this paper, we propose a new method for unmixing of hyperspectral images in Bayesian sense referred to as the normal compositional model with the sparse Dirichlet prior (NCM-SDP). We consider a semi-supervised scenario with the NCM and use the Dirichlet prior to represent the abundance vector sparsity. The Markov Chain Monte Carlo (MCMC) sampler is used to generate posteriors.

2 NCM-SDP method

To introduce the proposed NCM-SDP method, we elaborate on the NCM definition, prior selection, and the posterior derivation as follows.

2.1 Normal compositional model

In mixing approaches, the spectral variation of endmembers is randomly defined as:

$$\boldsymbol{e_r} \sim \mathcal{F}\left(.|\boldsymbol{\theta}_r\right), \tag{1}$$

where $\mathcal{F}$ shows the conditional probability density function (pdf) of a material and $\boldsymbol{\theta}_r$ is the vector of hyper parameters of the distribution corresponding to the rth endmember. Also, a random vector of L-spectral band pixel $\boldsymbol{y} = [y_1, \ldots, y_L]^T$ with a stochastic linear mixture of endmembers is given by [18]:

$$\boldsymbol{y} = \sum_{r=1}^{R} \boldsymbol{e}_r \alpha_r, \tag{2}$$

where $\boldsymbol{e}_r$ is the spectral signature of the rth endmember defined by (1), R is the number of endmembers, and α_r denotes the abundance of the rth endmember. To define each endmember in Bayesian sense, the Gamma and beta priors have already been applied [18,19]. In such cases, however, the exact knowledge of endmember distributions is required, which may not be available in practice. The Gaussian distribution may also be considered in which the unknown parameters can be jointly estimated together with the abundance fractions. In the NCM, endmembers are defined by independent multivariate Gaussian vectors. We assume that the mean of each endmember is known and the covariance matrix of endmembers can be written as a scalar matrix. The pdf of the rth endmember is defined as:

$$\boldsymbol{e}_r \sim \mathcal{N}\left(\boldsymbol{m}_r, \sigma^2 \boldsymbol{I}_L\right), \tag{3}$$

where $\boldsymbol{m}_r = \left[m_{r,1}, \ldots, m_{r,L}\right]^T$ is the known mean of $\boldsymbol{e}_r$ for $r = 1, \ldots, R$, $\boldsymbol{I}_L$ is an $L \times L$ identity matrix, and σ^2 shows the unknown variance of endmembers in each spectral band. Since the endmembers spectra are independent from each other, the likelihood function of each hyperspectral mixed pixel is expressed as:

$$f\left(\boldsymbol{y}|\boldsymbol{\alpha}, \sigma^2\right) = \frac{1}{\left(2\pi\sigma^2 c\left(\boldsymbol{\alpha}\right)\right)^{L/2}} \exp\left(-\frac{\|y - \mu\left(\boldsymbol{\alpha}\right)\|_2^2}{2\sigma^2 c\left(\boldsymbol{\alpha}\right)}\right), \tag{4}$$

where $\|\cdot\|_2$ defines the standard ℓ_2 norm, $c\left(\boldsymbol{\alpha}\right) = \sum_{r=1}^{R} \alpha_r^2$, $\mu(\boldsymbol{\alpha}) = \sum_{r=1}^{R} \boldsymbol{m}_r \alpha_r$, and $\boldsymbol{\alpha} = [\alpha_1, \ldots, \alpha_R]^T$ shows the abundance vector. Using a hierarchical Bayesian algorithm, the unknown parameters $\boldsymbol{\alpha}$ and σ^2 are estimated.

2.2 Prior selection

2.2.1 Endmember variance prior

As in [12], a conjugate inverse gamma distribution is chosen as a prior distribution for the endmember variance as:

$$f\left(\sigma^2|\delta\right) \sim \mathcal{IG}\left(\nu, \delta\right), \tag{5}$$

where ν and δ show the shape and scale parameters, respectively. We assume $\nu = 1$, and the hyperparameter δ is defined by the non-informative Jeffreys' prior as:

$$f\left(\delta\right) \sim \frac{1}{\delta} 1_{\mathbb{R}^+}\left(\delta\right), \tag{6}$$

where $1_{\mathbb{R}^+}(.)$ is the indicator function defined on $\mathbb{R}^+$ as:

$$1_{\mathbb{R}^+}(\delta) = \begin{cases} 1, & \text{if } \delta \in \mathbb{R}^+; \\ 0, & \text{otherwise.} \end{cases} \tag{7}$$

2.2.2 Abundance prior

The abundance vector should be estimated under the non-negativity and sum-to-one constraints shown as:

$$\alpha_r \geq 0, \quad r = 1, \ldots, R, \qquad \sum_{r=1}^{R} \alpha_r = 1. \tag{8}$$

Then, the fractional abundance vector $\boldsymbol{\alpha}$ will be in the standard $(R-1)$-simplex. Under such circumstances, choosing an appropriate prior for the abundance vector becomes harder. To fulfill the above constraints, in most recent works the uniform distribution is considered over a set of fractional values [11]. However, since the number of endmembers contributing in a mixed pixel is usually much smaller than that

of the dictionary, this distribution cannot describe the abundance vector properly. In turn, we may exploit the sparse property of the abundance vector due to its small number of nonzero elements [19].

In this paper, we propose the symmetric Dirichlet distribution as the abundance prior defined as [20]:

$$f(\boldsymbol{\alpha}) \sim \mathcal{D}(\boldsymbol{\alpha};\beta) = \frac{\Gamma(\beta R)}{\Gamma(\beta)^R} \prod_{r=1}^{R} \alpha_r^{\beta-1}, \tag{9}$$

where $\Gamma(\cdot)$ is the Gamma function and β determines the concentration of the Dirichlet distribution and accordingly the abundance vector sparsity. This distribution satisfies the abundance vector non-negativity and sum-to-one constraints. For $\beta = 1$, it corresponds to the uniform distribution over the standard $(R-1)$-simplex, and for $\beta > 1$, becomes denser around its mean. On the other hand, for $\beta < 1$, the Dirichlet prior tends to concentrate close to zero in which case most of the elements of $\boldsymbol{\alpha}$ would be extremely small. This case can properly describe the sparse behavior of an abundance vector in a *semi-supervised* scenario. Clearly, if the uniform prior ($\beta = 1$), which would be more appropriate for a *supervised* scheme, as used in [11–13], is applied to a *semi-supervised* scheme, we might encounter with large unmixing errors. Here, we consider a *semi-supervised* scheme which is more encountered in practice and propose to incorporate the sparse Dirichlet prior, and we will show its outperformance later.

2.3 Derivation of posterior distribution

Based on Bayes' theorem, the joint posterior distribution of the unknown variables is defined as:

$$f\left(\boldsymbol{\alpha}, \sigma^2, \delta | \boldsymbol{y}\right) \propto f\left(\boldsymbol{y}|\boldsymbol{\alpha}, \sigma^2\right) f\left(\boldsymbol{\alpha}, \sigma^2|\delta\right) f(\delta), \tag{10}$$

where by assuming independency between unknown parameters, we get $f\left(\boldsymbol{\alpha}, \sigma^2|\delta\right) = f(\boldsymbol{\alpha}) f\left(\sigma^2|\delta\right)$. Then, by using (4), (5), (6), and (9) in (10), $f\left(\boldsymbol{\alpha}, \sigma^2, \delta|\boldsymbol{y}\right)$ is obtained as:

$$f\left(\boldsymbol{\alpha}, \sigma^2, \delta|\boldsymbol{y}\right) \propto \frac{\mathbf{1}_{\mathcal{R}^+}(\delta) \prod_{r=1}^{R} \alpha_r^{\beta-1}}{\left(\sigma^2 c(\boldsymbol{\alpha})\right)^{\frac{L}{2}} \sigma^2} \times \exp\left(-\frac{\|y - \mu(\boldsymbol{\alpha})\|^2}{2\sigma^2 c(\boldsymbol{\alpha})} - \delta\right). \tag{11}$$

Due to the complexity of (11), it is intractable to obtain the MMSE or MAP estimates in closed form for the abundances and endmember variance. A solution is to generate the samples according to (11) and then to approximately apply Bayesian estimators to these samples [21].

3 MCMC sampling

The MCMC methods are used for iterative sampling from a probability distribution based on generating a Markov chain [21]. To do so, we should derive $f\left(\boldsymbol{\alpha}|\boldsymbol{y}, \sigma^2\right)$, $f\left(\sigma^2|\boldsymbol{y}, \boldsymbol{\alpha}, \delta\right)$, and $f\left(\delta|\sigma^2\right)$ to estimate the unknown parameters α, σ^2, and the unknown hyperparameter δ. Using (4) and (9) in the Bayes' theorem, the posterior $f(\boldsymbol{\alpha}|\boldsymbol{y}, \sigma^2)$ is given by:

$$f\left(\boldsymbol{\alpha}|\boldsymbol{y}, \sigma^2\right) \propto \frac{1}{\left(\sigma^2 c(\boldsymbol{\alpha})\right)^{\frac{L}{2}}} \times \exp\left(-\frac{\|\boldsymbol{y} - \mu(\boldsymbol{\alpha})\|^2}{2\sigma^2 c(\boldsymbol{\alpha})}\right) \prod_{r=1}^{R} \alpha_r^{\beta-1}. \tag{12}$$

According to (12), the samples of abundance vector are generated using the MCMC [12]. Using (4), (5), and (6), the posteriors of σ^2 and δ are also calculated, respectively, as:

$$f\left(\sigma^2|\boldsymbol{y}, \boldsymbol{\alpha}, \delta\right) \propto \mathcal{IG}\left(\frac{L}{2} + 1, \frac{\|\boldsymbol{y} - \mu(\boldsymbol{\alpha})\|^2}{2c(\boldsymbol{\alpha})} + \delta\right), \tag{13}$$

and

$$f\left(\delta|\sigma^2\right) \propto \mathcal{G}\left(1, \frac{1}{\sigma^2}\right). \tag{14}$$

The required procedure for using the NCM-SDP is summarized in Alg. 1.

Algorithm 1. NCM-SDP procedure.

1. Input vectors: $[\boldsymbol{y}_1,...,\boldsymbol{y}_N]$, $[\boldsymbol{e}_1,...,\boldsymbol{e}_R]$
2. Output estimates: $\hat{\boldsymbol{\alpha}}$, $\hat{\sigma}^2$
3. Initialization:
   a. Sample $\delta(0)$
   b. Sample $\sigma(0)$
4. Iterations:
   a. Sample $\boldsymbol{\alpha}(t)$ according to (12) using MCMC
   b. Sample $\sigma^2(t)$
   c. Sample $\sigma(t)$

4 Experimental results

To evaluate the performance of the NCM-SDP, our experiments are performed on both simulated and real hyperspectral images as follows.

4.1 Simulated data

We first compare the performance of the NCM-SDP method to that of the classical Bayesian NCM algorithm with the

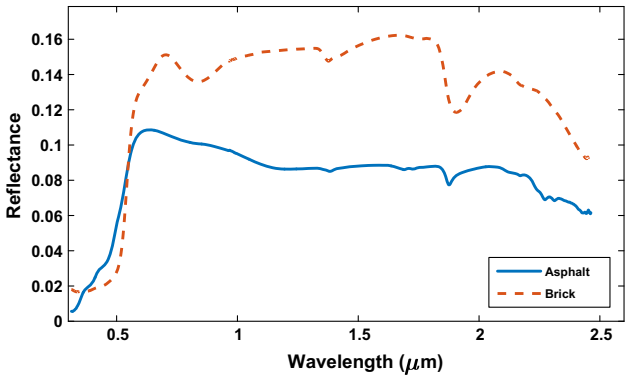

Fig. 1 Endmember spectral signatures for "asphalt" and "brick"[22]

uniform prior [12], which we call the "NCM uniform." Ten endmembers are randomly selected from the USGS digital spectral library each one consisting of 2151 spectral bands in the wavelength range of 0.35–2.5 μm [22] to build up our spectral dictionary. The materials are "asphalt," "brick," "cedar," "concrete," "fabric," "fiberglass," "nylon," "pipe," "plastic," and "polyester." Hyperspectral pixels are mixed of asphalt and brick shown in Fig. 1 with proportions [0.3, 0.7]. Then, $\boldsymbol{\alpha} = [0.3, 0.7, 0, 0, 0, 0, 0, 0, 0, 0]$ shows the abundance vector with the sparsity level of 0.2. Also, the endmembers variance is set to $\sigma^2 = 0.05$ for all spectral bands of all 10 endmembers.

To choose a proper value of β in the NCM-SDP, we repeat the unmixing algorithm for $0 \leq \beta \leq 1$ and compare the absolute values of the abundance estimation errors using:

$$|e| = \|\alpha_r - \hat{\alpha}_r\|_1. \tag{15}$$

where $\hat{a}_r$ denotes the MAP abundance estimate of the rth endmember.

To define the sparsity level, we generate thousands of Dirichlet distributed samples for each specified β and consider the percentage of significant values to the whole number of samples.

The results shown in Table 1 clearly show a salient reduction in $|e|$ for the smaller values of β. However, note that, in practice, the number of participant endmembers for modeling of a hyperspectral pixel is unknown, a priori, and choosing a very small β can lead to a large error. In fact, there is a trade-off between the sparsity level of the prior and the generated abundance estimation error. By including these considerations, we have chosen $\beta = 0.1$ and later will show that this value is appropriate for our unmixing problem. Note that for different sizes of dictionaries, proper values of β should be reselected correspondingly. This subject can be regarded as an open problem for future research.

For $\beta = 0.1$, the posteriors of abundances are generated by the NCM-SDP method for 300 independent trials

Table 1 Abundance estimation errors for different β's

β	0.001	0.01	0.05	0.1	0.2	0.5	1
Sparsity level	0.01	0.04	0.12	0.18	0.24	0.32	0.37
$\|e\|$	0.05	0.04	0.08	0.06	0.13	0.27	0.42

of the experiment. The averages of the generated posteriors for the first and second abundances are illustrated in Fig. 2a, b, respectively. Considering that α contains 10 entries, in Fig. 2c, we have only shown the distribution of the third entry which is very similar to those of the fourth to tenth ones. As seen, the peaks of the posteriors obtained from the NCM-SDP are more concentrated around the real values.

From the MAP estimation theory, the first and second abundances are estimated as 0.31 and 0.68, respectively, which are very close to the corresponding real values in $\boldsymbol{\alpha}$, i.e., 0.3, and 0.7. These estimates from the NCM uniform [12] are 0.47 and 0.47, respectively, showing the lower accuracy of the method. Moreover, for the other 8 entries of $\boldsymbol{\alpha}$ (zero values), the NCM-SDP generates negligible values of order 10^{-11}, while they are of order 10^{-4} for [12]. Also, the values of $|e|$ achieved by the NCM-SDP and [12] are 0.137 and 0.484, respectively. This enhancement is effectively achieved due to applying the Dirichlet prior with a proper value of β.

Next, the posteriors of the variance of endmembers estimated based on the Gaussian prior are plotted in Fig. 3. As seen, the resulted posterior by the NCM-SDP is much closer to the real value compared to that of [12] which logically leads to a lower estimation error.

4.2 Real hyperspectral data

The performance of NCM-SDP is now compared to that of [12] for the real hyperspectral image shown in Fig. 4a. This image has been collected by the airborne visible/infrared imaging spectrometer (AVIRIS) over Cuprite, Nevada, USA [23]. A square patch of 50×50 pixel of the image is cropped as the region of interest (ROI), as shown in Fig. 1b. The reconstructed images using the NCM uniform and NCM-SDP methods are shown in Fig. 4c, d, respectively.

By comparing Fig. 4c, d to b, one can observe that the NCM-SDP reconstructs the real image more similarly. To inspect this matter quantitatively, the MSEs of both methods are shown in Table 2 using (16).

$$\text{MSE} = \frac{1}{N}\sum_{n=1}^{N}\left\|\boldsymbol{y}_n - \sum_{r=1}^{R}\boldsymbol{e}_r\alpha_{r,n}\right\|_2^2 \tag{16}$$

To more evaluate the NCM-SDP, in another experiment, we utilize the real data set "Gulfport hyperspectral image" collected from Long beach MS [11]. A block of 13×19 pixel

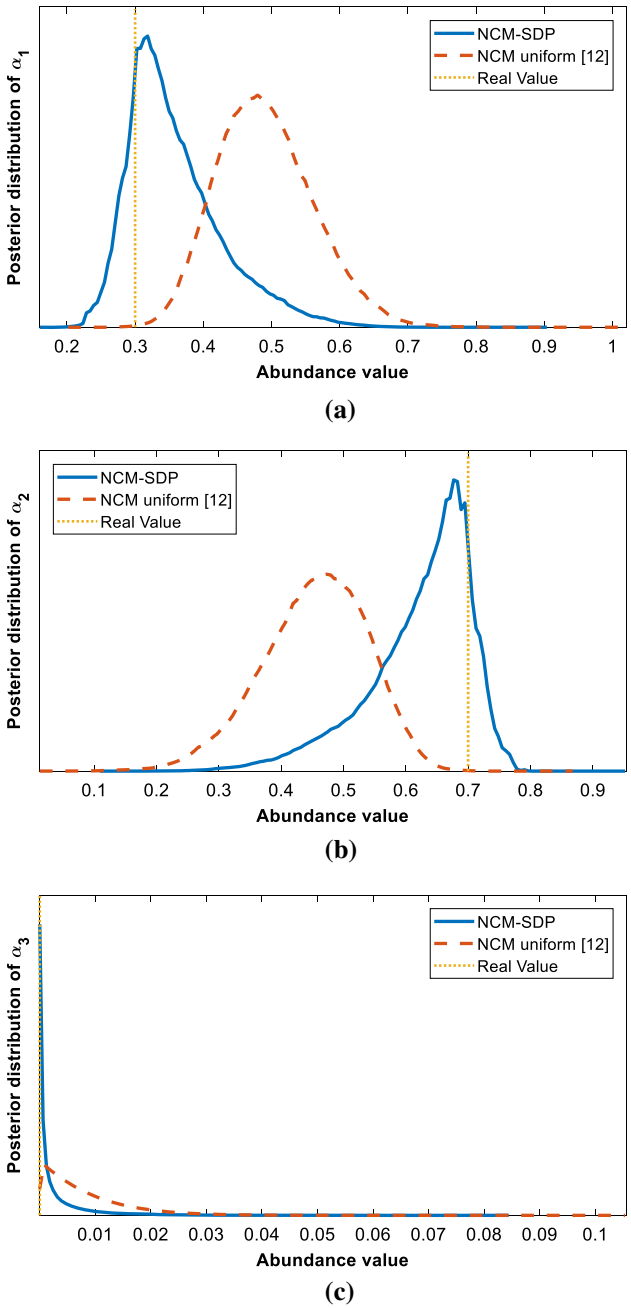

Fig. 2 Estimated posteriors of the **a** first, **b** second, and **c** third abundance values

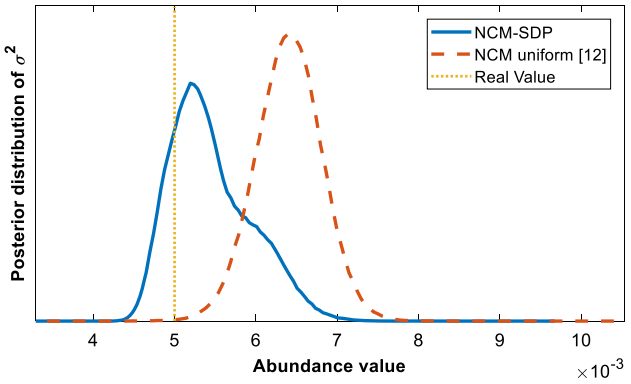

Fig. 3 Estimated posteriors of the variance of endmembers

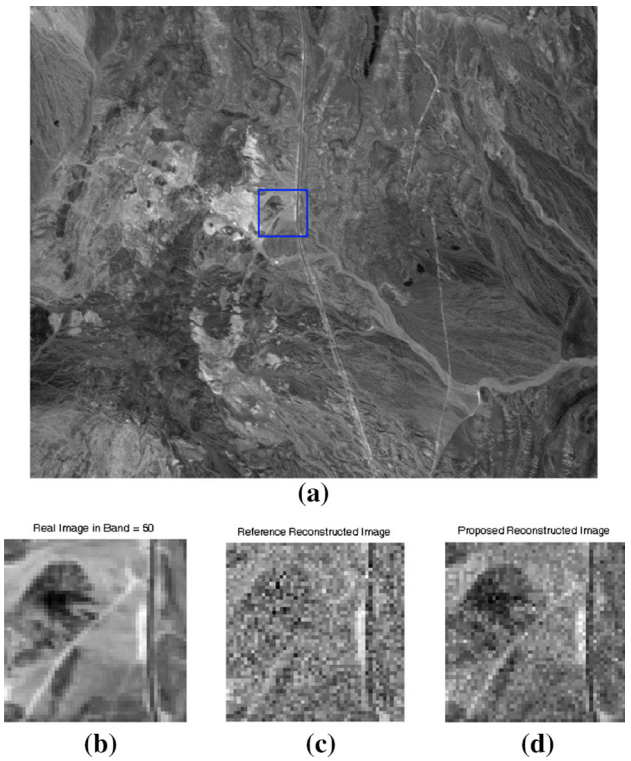

Fig. 4 **a** Cuprite image [23], **b** ROI, **c** reconstructed image by [12], and **d** reconstructed image by the NCM-SDP

Table 2 MSEs of reconstructed images

	NCM uniform [12]	NCM-SDP
MSE	1.94	**1.52**

Proposed result shown in bold

of this image is cropped for which the accurate endmembers are available. Also, for each endmember of this region, there exist 10 different samples. Note that for the NCM-SDP, only one of these samples is sufficient to be used as the mean of that endmember signature, while for the BCM algorithms more samples are needed for extraction of the beta distribution parameter. Here, we use the average of samples as the mean of each Gaussian distributed endmember. NCM-SDP is compared to the FCLS [24], BCM QP [25], BCM sampling [25], BCM-spatial QP [11], BCM-spatial sampling [11], NCM QP [10], NCM sampling [10], and NCM uniform [12].

The maps of estimated abundances for 4 endmembers are depicted in Fig. 5. We use the ground truth of data addressed in [11] for 4 endmembers including "asphalt," "yellow curb," "grass," and "oak leaves" as shown in Fig. 5j, respectively.

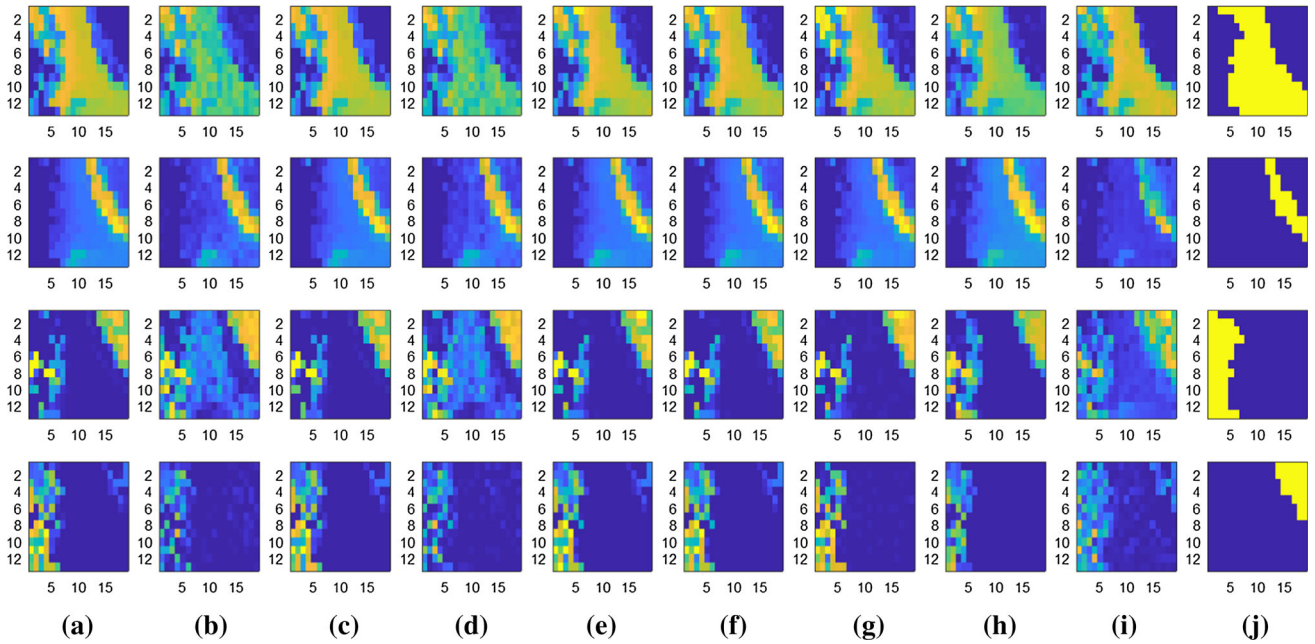

Fig. 5 Abundance maps of "asphalt," "yellow curb," "grass," and "oak leaves" in the Gulfport image for **a** FCLS, **b** BCM-spectral QP, **c** BCM-spectral sampling, **d** BCM-spatial QP, **e** BCM-spatial sampling, **f** Gaussian QP, **g** Gaussian sampling, **h** NCM uniform, **i** NCM-SDP, and **j** ground truth

In each figure, the yellow and blue parts correspond to the abundance values equal to 1 and 0, respectively. For a better evaluation, the average per pixel per endmember proportion error is defined as [11]:

$$\text{PError} = \frac{1}{\text{NR}} \sum_{n=1}^{N} \|\boldsymbol{\alpha}_n - \hat{\boldsymbol{\alpha}}_n\|_2 \tag{17}$$

where $\boldsymbol{\alpha}_n$ is the true abundance vector of pixel n, $\boldsymbol{\alpha}_n$ is the corresponding estimated abundance vector, N shows the number of pixels, and R is the number of endmembers. Each method is run 10 times, and the average of total errors is calculated. The results are presented in Table 3. It is vital to note that in this experiment all the above comparative methods are *supervised* schemes with a dictionary of 4 endmembers as opposed to the NCM-SDP which is a *semi-supervised* scheme with 30 endmembers in the dictionary. It is interesting to note that although this scenario is intrinsically appropriate for *supervised* cases, still the corresponding techniques are unable to reconstruct the images as accurate as the NCM-SDP. From Table 3, one can conclude that the NCM-SDP has estimated the abundance vector more accurately than the BCM- and NCM-based unmixing methods.

All the enhanced results achieved by the NCM-SDP reveal that incorporation of the sparse property of abundance vectors based on the sparse Dirichlet prior into the mixing model is a rational and realistic proposition.

Table 3 Average per pixel per endmember proportion error for the Gulfport hyperspectral image

Method	PError
FCLS [24]	0.1527
BCM-spectral quadprog [25]	0.1497
BCM-spectral sampling [25]	0.1498
BCM-spatial quadprog [11]	0.1507
BCM-spatial sampling [11]	0.1433
NCM quadprog [10]	0.1517
NCM sampling [10]	0.1619
NCM uniform [12]	0.1425
NCM-SDP	**0.1325**

Proposed result shown in bold

5 Conclusions

A new hierarchical Bayesian method was derived for unmixing of hyperspectral images. Endmembers were considered variable based on the Gaussian distribution. Also, we assumed that the abundance vectors are sparse. The sparse Dirichlet prior was proposed for sparse modeling and accordingly the NCM-SDP method was developed. Using the simulated data, it was shown that the error of the estimated abundance vector is approximately 7 times smaller than that of the uniform prior. Also, by repeating the simulations for real data, 20% improvement in the MSE sense was achieved.

References

1. Plaza, A., Benediktsson, J.A., Boardman, J., Brazile, J., Bruzzone, L., Camps-Valls, G., Chanussot, J., Fauvel, M., Gamba, P., Gualtieri, J., Marconcini, M., Tilton, J.C., Trianni, G.: Recent advances in techniques for hyperspectral image processing. Remote Sens. Environ. **113**(1), 110–122 (2009)
2. Somers, B., Delalieux, S., Stuckens, J., Verstraeten, W.W., Coppin, P.: A weighted linear spectral mixture analysis approach to address endmember variability in agricultural production systems. Int. J. Remote Sens. **30**(1), 139–147 (2009)
3. Settle, J.J., Drake, N.A.: Linear mixing and the estimation of ground cover proportions. Int. J. Remote Sens. **14**(6), 1159–1177 (1993)
4. Chang, C.I., Heinz, D.C.: Constrained subpixel target detection for remotely sensed imagery. IEEE Trans. Geosci. Remote Sens. **38**(3), 1144–1159 (2000)
5. Vane, G., Green, R., Chrien, T., Enmark, H., Hansen, E., Porter, W.: The airborne visible/infrared imaging spectrometer (AVIRIS). Remote Sens. Environ. **44**(2–3), 127–143 (1993)
6. Keshava, N., Mustard, J.F.: Spectral unmixing. IEEE Signal Proc. Mag. **19**(1), 44–57 (2002)
7. Bateson, C., Asner, G., Wessman, C.: Endmember bundles: a new approach to incorporating endmember variability into spectral mixture analysis. IEEE Trans. Geosci. Remote Sens. **38**(2), 1083–1094 (2000)
8. Zare, A., Ho, K.C.: Endmember variability in hyperspectral analysis. IEEE Signal Proc. Mag. **31**(1), 95–104 (2014)
9. Mianji, F., Zhang, Y.: SVM-based unmixing-to-classification conversion for hyperspectral abundance quantification. IEEE Trans. Geosci. Remote Sens. **49**(11), 4318–4327 (2011)
10. Stein, D.: Application of the normal compositional model to the analysis of hyperspectral imagery. In: Proceedings of Workshop Advances in Techniques for Analysis Remotely Sensed Data, pp. 44–51. Greenbelt, USA (2003)
11. Du, X., Zare, A., Gader, P., Dranishnikov, D.: Spatial and spectral unmixing using the beta compositional model. IEEE J. Sel. Top. Appl. Earth Obs. **7**(6), 1994–2002 (2014)
12. Eches, O., Dobigeon, N., Mailhes, C., Tourneret, J.Y.: Bayesian estimation of linear mixtures using the normal compositional model. Application to hyperspectral imagery. IEEE Trans. Image Process. **19**(6), 1403–1413 (2010)
13. Zare, A., Gader, P., Casella, G.: Sampling piecewise convex unmixing and endmember extraction. IEEE Trans. Geosci. Remote Sens. **51**(3), 1655–1665 (2013)
14. Ülkü, I., Töreyin, B.U.: Sparse coding of hyperspectral imagery using online learning. Signal Image Video Proc. **9**(4), 959–966 (2015)
15. Thouvenin, P.A., Dobigeon, N., Tourneret, J.Y.: Hyperspectral unmixing with spectral variability using a perturbed linear mixing model. IEEE Trans. Signal Proc. **64**(2), 525–538 (2016)
16. Peng, J., Luo, T.: Sparse matrix transform-based linear discriminant analysis for hyperspectral image classification. Signal Image Video Process. **10**(4), 761–768 (2016)
17. Uezato, T., Murphy, R.J., Melkumyan, A., Chlingaryan, A.: A novel spectral unmixing method incorporating spectral variability within endmember classes. IEEE Trans. Geosci. Remote Sens. **54**(5), 2812–2831 (2016)
18. Eismann, M.T., Stein, D.: Stochastic mixture modeling in hyperspectral data exploitation: theory and applications, Ch 5. In: Chang, C.I. (ed.) Wiley, New York (2007)
19. Guo, Z., Wittman, T., Osher, S.: L1 unmixing and its application to hyperspectral image enhancement. In: Proceedings of the SPIE,**7334**, pp. 1-9. Orlando, USA (2009)
20. Ng, K.W., Tian, G.L., Tang, M.L.: Dirichlet and Related Distributions: Theory, Methods and Applications. Wiley, New York (2011)
21. Robert, C.P., Casella, G.: Monte Carlo Statistical Methods, 2nd edn. Springer, New York (2004)
22. http://speclab.cr.usgs.gov/spectral-lib.html [Online]. Accessed May 2016
23. Swayze, G., Clark, R., Sutley, S., Gallagher, A.: Ground-truthing AVIRIS mineral mapping at Cuprite, Nevada. In: Proceedings of the Summaries 3rd Annual JPL Airborne Geosci. Workshop, pp. 47–49 (1992). https://aviris.jpl.nasa.gov/data/free_data.html. Accessed May 2016
24. Heinz, D., Chang, C.I.: Fully constrained least squares linear spectral mixture analysis method for material quantification in hyperspectral imagery. IEEE Trans. Geosci. Remote Sens. **39**(3), 529–545 (2001)
25. Zare, A., Gader, P., Drashnikov, D., Glenn, T.: Beta compositional model for hyperspectral unmixing. In: Proceedings of the 5th Workshop Hyperspectral Image Signal Processing: Evolution Remote Sensing, Gainesville, USA (2013)